Polyiron Oxo Chemistry at the Molecular/Solid-State Boundary: Synthesis, Structure, and Magnetic and Mössbauer Properties of $[Fe_{16}MO_{10}(OH)_{10}(O_2CPh)_{20}]$ Complexes, M = Mn, Fe, or Co

Wolfgang Micklitz,[1] Vickie McKee,[1] R. Lynn Rardin,[1] Laura E. Pence,[1] Georgia C. Papaefthymiou,[2] Simon G. Bott,[1] and Stephen J. Lippard*,[1]

Contribution from the Department of Chemistry and the Francis Bitter National Magnet Laboratory, Massachusetts Institute of Technology, Cambridge, Massachusetts 02139

Received March 14, 1994®

Abstract: Three polyiron complexes of general formula $[Fe_{16}MO_{10}(OH)_{10}(O_2CPh)_{20}]$, where M = Mn (**1**), Fe (**2**), or Co (**3**), have been synthesized from the triiron precursors $[Fe_3O(O_2CPh)_6(H_2O)_2(MeCN)]$ and $[Fe_3O(O_2CPh)_6(Me_2O)_3](O_2CPh)$. The heptadecanuclear compounds crystallize from acetonitrile/water solutions in low to modest yields, the major product being the known undecanuclear cluster $[Fe_{11}O_6(OH)_6(O_2CPh)_{15}]$. Compounds **1-3** have been characterized by single-crystal X-ray structure determinations. In each case, the heteroatom M is located on a center of symmetry within the compact $Fe_{16}MO_{10}(OH)_{10}$ cluster, which is, in turn, encapsulated by the 20 coordinated benzoate anions. The polymetallic clusters in the heptadecanuclear complexes can be formally constructed by fusion of two fragments generated from the $\{Fe_{11}O_6(OH)_6\}$ core of the undecanuclear molecule. All the metal ions have distorted octahedral geometry. Low-temperature Mössbauer spectroscopic and magnetic studies revealed properties normally associated with solid-state infinite arrays so that these complexes may be described as straddling the molecular/solid-state boundary. Specifically, at low temperature, both **1** and **2** exhibit Mössbauer spectra in zero and externally applied fields consistent with the onset of cooperative magnetic interactions arising from short-range ordering within the multinuclear spin structure. In addition, there is a rapid decrease in magnetic moment at low temperature, indicating that the magnetic interactions are antiferromagnetic in nature. Similar properties have been reported for polynuclear Fe(III)-apoferritin complexes formed at the initial stage of iron nucleation on the surface of the ferritin cavity.

Introduction

A decade ago the structurally characterized polyiron oxo complexes were limited to basic iron carboxylates and simple μ-oxodiiron(III) species.[3,4] In the ensuing years, the controlled synthesis of polyiron oxo-hydroxo clusters has become a subject of considerable interest because such units may resemble intermediates involved in the biological storage, detoxification, and recycling of iron. A key component in these processes is the iron storage protein ferritin (Ft), found in bacteria, plants, and animals. Ft is comprised of 24 subunits which form a hollow sphere with an internal diameter of 80 Å that can store up to 4500 iron atoms.[5-9] Less reversible formation of iron oxo-hydroxo deposits occurs in some species by the process of biomineralization,[10] a recent spectacular manifestation of which is the reported formation of magnetite in the human brain.[11] Apart from these biological phenomena, interest in polyiron oxo chemistry has been stimulated by the desire to exploit the properties of nanometer-sized structures and understand the transition from the molecular to the solid state.[12,13]

Since 1984, the development of a variety of synthetic strategies for controlled polymerization of iron in nonaqueous media has yielded structurally characterized complexes of nuclearity Fe_4,[14-18] Fe_6,[19-23] Fe_8,[24] Fe_{10},[25] Fe_{11},[26] Fe_{12},[27] Fe_{17},[28] and Fe_{19}.[28] In many of these complexes,[15,16,19-21,24-26] $\{Fe_2O\}$, $\{Fe_3O\}$, $\{Fe_4O_2\}$, and $\{Fe_6O\}$ are recurring structural features (Figure 1), and it is attractive to regard the clusters as being formally constructed from such units.[4,27,29] Most often, the synthetic route to these building blocks has involved hydrolytic polymerization, although recently slow oxidation of an iron(II) precursor with dioxygen has been employed.[27] The mechanisms of these polymerization reactions are not well understood, however.

In the present article we describe our studies of $[Fe_{16}MO_{10}(OH)_{10}(O_2CPh)_{20}]$ molecules, hereafter abbreviated $\{Fe_{16}M\}$, where M = Mn (**1**), Fe (**2**), or Co (**3**). Although some of the

* Abstract published in *Advance ACS Abstracts*, July 15, 1994.

(1) Department of Chemistry.
(2) Francis Bitter National Magnet Laboratory.

(3) Lippard, S. J. *Chem. Br.* **1986**, *22*, 222.
(4) Lippard, S. J. *Angew. Chem., Int. Ed. Engl.* **1988**, *27*, 344.
(5) Crichton, R. R. *Angew. Chem., Int. Ed. Engl.* **1973**, *12*, 57.
(6) Theil, E. C. *Adv. Inorg. Biochem.* **1983**, *5*, 1.
(7) Rice, D. W.; Ford, G. C.; White, J. L.; Smith, J. M. A.; Harrison, P. M. *Adv. Inorg. Biochem.* **1983**, *5*, 39.
(8) Ford, G. C.; Harrison, P. M.; Rice, D. W.; Smith, J. M. A.; Treffry, A.; White, J. L.; Yariv, J. *Philos. Trans. R. Soc. London, B* **1984**, *304*, 551.
(9) Harrison, P. M.; Andrews, S. C.; Artymiuk, P. J.; Ford, G. C.; Guest, J. R.; Hirzmann, J.; Lawson, D. M.; Livingstone, J. C.; Smith, J. M. A.; Treffry, A.; Yewdall, S. J. *Adv. Inorg. Chem.* **1991**, *36*, 449.
(10) Mann, S. *Endeavour* **1991**, *15*, 120.
(11) Kirschvink, J. L.; Kobayashi-Kirschvink, A.; Woodford, B. J. *Proc. Natl. Acad. Sci. U.S.A.* **1992**, *89*, 7683.
(12) Ziolo, R. F.; Giannelis, E. P.; Weinstein, B. A.; O'Horo, M. P.; Ganguly, B. N.; Mehrotra, V.; Russell, M. W.; Huffman, D. R. *Science* **1992**, *257*, 219.
(13) Papaefthymiou, G. C. *Phys. Rev. B* **1992**, *46*, 10366. Papaefthymiou, G. C. In *On Clusters and Clustering: From Atoms to Fractals*; Reynolds, P. J., Ed.; Elsevier Science Publishers: Amsterdam, 1993; p 209.
(14) Stukan, R. A.; Ponomarev, V. I.; Nifontov, V. P.; Turté, K. I.; Atovmyan, L. O. *Zh. Strukt. Khim.* **1985**, *26*, 197.
(15) Armstrong, W. H.; Roth, M. E.; Lippard, S. J. *J. Am. Chem. Soc.* **1987**, *109*, 6318.
(16) Gorun, S. M.; Lippard, S. J. *Inorg. Chem.* **1988**, *27*, 149.
(17) Murch, B. P.; Bradley, F. C.; Boyle, P. D.; Papaefthymiou, V.; Que, L., Jr. *J. Am. Chem. Soc.* **1987**, *109*, 7993.
(18) Jameson, D. L.; Xie, C.-L.; Hendrickson, D. N.; Potenza, J. A.; Schugar, H. J. *J. Am. Chem. Soc.* **1987**, *109*, 740.
(19) Gerbeleu, N. V.; Batsanov, A. S.; Timko, G. A.; Struchkov, Y. T.; Indrichan, K. M.; Popovich, G. A. *Dokl. Akad. Nauk SSSR* **1986**, *293*, 364.
(20) Micklitz, W.; Lippard, S. J. *Inorg. Chem.* **1988**, *27*, 3067.
(21) Micklitz, W.; Bott, S. G.; Bentsen, J. G.; Lippard, S. J. *J. Am. Chem. Soc.* **1989**, *111*, 372.
(22) Nair, V. S.; Hagen, K. S. *Inorg. Chem.* **1992**, *31*, 4048.
(23) Hegetschweiler, K.; Schmalle, H. W.; Streit, H. M.; Gramlich, V.; Hund, H.-U.; Erni, I. *Inorg. Chem.* **1992**, *31*, 1299.
(24) Wieghardt, K.; Pohl, K.; Jibril, I.; Huttner, G. *Angew. Chem., Int. Ed. Engl.* **1984**, *23*, 77.
(25) Taft, K. L.; Lippard, S. J. *J. Am. Chem. Soc.* **1990**, *112*, 9629.

0002-7863/94/1516-8061$04.50/0

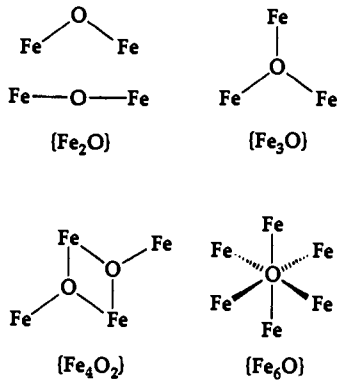

Figure 1. Structures of common building blocks encountered in synthetic polyiron oxo cores.

properties of these compounds have been previously communicated,[13,30,31] we report here the details of their preparation, structures, and Mössbauer and magnetic properties, including for the first time the synthesis and structure of **2**. As will be shown, the $\{Fe_{16}M\}$ molecules are formally comprised of two fragments of the well-studied $[Fe_{11}O_6(OH)_6(O_2CPh)_{15}]$ compound,[26] designated $\{Fe_{11}\}$, which also exhibits interesting magnetic properties, albeit not superparamagnetism. These results, together with those of the recently discovered dodecairon oxo complex, $[Fe^{III}_4Fe^{II}_8(O)_2(OCH_3)_{18}(O_2CCH_3)_6(CH_3OH)_{4.67}]$ (**4**),[27] help to delineate the boundary between molecular and solid-state substances. In addition, we compare the properties of **1** and **2** with those recently reported for iron clusters bound to apoferritin.

Experimental Section

Preparation and Characterization of Compounds. Solvents and reagents were obtained from commercial sources and used without further purification. The starting material $[Fe_3O(O_2CPh)_6(Me_2O)_3](O_2CPh)$, $\{Fe_3O\}^{7+}$, was prepared by using a literature method.[32] IR spectra in the range 4000–400 cm^{-1} were recorded for KBr discs on a Mattson Cygnus 100 Fourier transform spectrometer.

$[Fe_3O(O_2CPh)_6(H_2O)_2(MeCN)]_2\{Fe_3O\}^{6+}$. A portion of $FeCl_2{\cdot}4H_2O$ (3.0 g, 0.015 mol) dissolved in 50 mL of deoxygenated water was added to a solution of 7.5 g (0.052 mol) of sodium benzoate in 100 mL of water. A pale precipitate formed at once, and the mixture was stirred in air for 1 h, followed by addition of 25 mL of acetonitrile. Some of the precipitate dissolved, and the suspension darkened to a brown color. Stirring was continued overnight, and the chocolate brown precipitate was filtered off and dried (4.7 g, 96% yield based on Fe). The dried complex was recrystallized from hot acetonitrile. Anal. Calcd for $C_{43}H_{37}Fe_3NO_{16}$: C, 53.53; H, 3.78; Fe, 16.97. Found: C, 53.45; H, 3.37; Fe, 17.44. FTIR (KBr): 1600, 1563, 1545, 1404, 1177, 1026, 840, 817, 720, 688, 674, 588, 540, 478 cm^{-1}.

$[Fe_{16}MnO_{10}(OH)_{10}(O_2CPh)_{20}]$ (1). Method A. To a suspension of $\{Fe_3O\}^{7+}$ (0.9 g, 0.77 mmol) in 30 mL of acetonitrile were added $Mn(ClO_4)_2{\cdot}6H_2O$ (0.2 g, 0.55 mmol) and 1.0 mL of water. The dark brown solution was refluxed for 30 min, then dried over molecular sieves or $MgSO_4$ for 2 h, and filtered. Crystalline samples (45 mg, 7.5% yield based on Fe) of $1{\cdot}2Et_2O{\cdot}3MeCN$ suitable for X-ray studies were obtained in several weeks by ether diffusion into the acetonitrile reaction mixture filtrate. Vacuum-dried samples were used for analysis. FTIR (KBr): 3952, 3559, 1598, 1542, 1419, 1178, 1025, 841, 828, 814, 715, 686, 678, 665, 604, 479 cm^{-1}. The same product can be obtained by allowing the dried solution to stand in a stoppered flask for 3–4 days. After 4–5 days, however, $[Fe_{11}O_6(OH)_6(OCPh)_{15}]{\cdot}H_2O{\cdot}8MeCN$, $\{Fe_{11}\}$, is also precipitated. The ether diffusion route avoids the problem of contamination by $\{Fe_{11}\}$. Anal. Calcd for $C_{140}H_{110}Fe_{16}MnO_{60}$: C, 45.44; H, 3.00; Fe, 24.14; Mn, 1.48. Found: C, 45.45; H, 3.05; Fe, 23.68; Mn, 1.56.

Method B. A solution of $\{Fe_3O\}^{7+}$ (0.9 g, 0.77 mmol) and $Mn(ClO_4)_2{\cdot}6H_2O$ (0.2 g, 0.55 mmol) in 25 mL of acetonitrile and 1.0 mL of water was refluxed for 24 h. After cooling, a dark brown powder was filtered off. The yield (100 mg, 18% based on Fe) was considerably higher than that obtained by method A; however, the Mössbauer data showed the presence of some iron-containing impurities in samples prepared by this method, and, since the product is not readily recrystallized, this route was not generally employed.

$[Fe_{16}FeO_{10}(OH)_{10}(O_2CPh)_{20}]$ (2). Method A. The mixed valence cluster $\{Fe_3O\}^{6+}$ was prepared as described above. After collection on a Buchner funnel, the partially dry $\{Fe_3O\}^{6+}$ was added to 150 mL of acetonitrile, and the mixture was boiled for 30 min to give a dark brown suspension. The suspension was allowed to cool, and unreacted $\{Fe_3O\}^{6+}$ was removed by filtration. Microcrystalline **2** was obtained by allowing the filtrate to stand open to air for 2 days. This reaction is very sensitive to the amount of water in the mixture, and yields are variable. In the best cases, ~60 mg of **2** was obtained (~2% yield based on Fe). The sample used for X-ray crystallography was obtained from a mixture of both **2** and $\{Fe_{11}\}$. Dark brown blocks of **2** were manually separated under a microscope from the long red-brown rods of $\{Fe_{11}\}$. FTIR (KBr): 3593, 3568, 1598, 1544, 1421, 1178, 1026, 842, 827, 814, 714, 686, 679, 668, 598, 477 cm^{-1}. Anal. Calcd for $C_{140}H_{110}Fe_{17}O_{60}$: C, 45.43; H, 3.00; N, 0.0. Found: C, 44.64; H, 2.96; N, <0.05.

Method B. Complex **2** can also be prepared in roughly the same yield by a method similar to that employed to synthesize **1**, with $\{Fe_3O\}^{6+}$ used in place of $\{Fe_3O\}^{7+}$ and $Fe(ClO_4)_2{\cdot}6H_2O$ replacing the manganese salt.

$[Fe_{16}CoO_{10}(OH)_{10}(O_2CPh)_{20}]$ (3). To a slurry of $\{Fe_3O\}^{7+}$ (0.9 g, 0.77 mmol) in 40 mL of acetonitrile were added 1.0 mL of water and $CoCl_2{\cdot}6H_2O$ (0.10 g, 0.42 mmol). The mixture was refluxed for 15 min, dried over $MgSO_4$, and then filtered. The green filtrate was allowed to stand in air, and dark brown crystals of **3**·17MeCN (50 mg, 9% yield based on Fe) formed within 48 h. FTIR (KBr): 3596, 3565, 1598, 1540, 1420, 1178, 1025, 842, 826, 812, 714, 686, 678, 665, 602, 480 cm^{-1}. Anal. Calcd for $C_{140}H_{110}CoFe_{16}O_{60}$: C, 45.39; H, 2.99. Found: C, 44.49; H, 2.82.

X-ray Crystallography. Single-crystal X-ray structural studies have been carried out on $1{\cdot}2Et_2O{\cdot}3MeCN$, **2**·18MeCN, and **3**·17MeCN by using methods previously reported.[33] In each case the data were collected on an Enraf-Nonius CAD4 diffractometer using graphite-monochromated Mo Kα radiation ($\bar{\lambda}$ = 0.71073 Å). The data sets were corrected for Lorentz and polarization effects and an empirical absorption correction was applied to the data. Experimental details are summarized in Table 1.

The structure of $1{\cdot}2Et_2O{\cdot}3MeCN$ was solved in the space group $P\bar{1}$ by using the direct methods option of SHELXS-86,[34] which revealed the positions of all the metal atoms and some of the oxygen atoms. The remaining non-hydrogen atoms were located on difference Fourier maps, and the structure was refined by least-squares methods with SHELXTL-PC.[35] One ether and two acetonitrile solvent molecules were located in the asymmetric unit, but one of the acetonitrile molecules was refined with site occupancy factors of 0.5. Anisotropic thermal parameters were assigned to the metal, oxygen, and non-hydrogen atoms of the full occupancy solvent molecules. Other atoms were refined with isotropic temperature factors. Hydrogen atoms were inserted at calculated positions. Those on hydroxide oxygen atoms coordinated to three iron atoms were inserted with tetrahedral geometry, whereas the proton on O10 (coordinated to Fe2 and Fe3 only) was inserted with planar geometry. Final refined positional and thermal parameters and full lists of bond distances and angles may be found in Tables S1–S3, respectively. Selected bond distances are presented in Table 2.

The direct methods option of SHELXS-86[34] was used to solve the structure of **2**·18MeCN in space group $P\bar{1}$. The initial solution revealed the positions of most of the non-hydrogen atoms, and alternating cycles of Fourier maps and least-squares refinement in TeXsan[36] were used to locate the remaining atoms. The asymmetric unit contains nine molecules of acetonitrile, all of which refined satisfactorily at full occupancy. All

(26) Gorun, S. M.; Papaefthymiou, G. C.; Frankel, R. B.; Lippard, S. J. *J. Am. Chem. Soc.* **1987**, *109*, 3337.
(27) Taft, K. L.; Papaefthymiou, G. C.; Lippard, S. J. *Science* **1993**, *259*, 1302.
(28) Heath, S. L.; Powell, A. K. *Angew. Chem., Int. Ed. Engl.* **1992**, *31*, 191.
(29) Hagen, K. S. *Angew. Chem., Int. Ed. Engl.* **1992**, *31*, 1010.
(30) Micklitz, W.; Lippard, S. J. *J. Am. Chem. Soc.* **1989**, *111*, 6856.
(31) Papaefthymiou, G. C. In *Nanophase and Nanocomposite Materials*; Komarneni, S., Parker, I. C., Thomas, G. J., Eds.; MRS Symposium Proceedings; Materials Research Society: Pittsburgh, PA, Vol. 286, 1993; p 67.
(32) Weinland, R. F.; Herz, A. *Ber. Dtsch. Chem. Ges.* **1912**, *45*, 2662.
(33) Carnahan, E. M.; Rardin, R. L.; Bott, S. G.; Lippard, S. J. *Inorg. Chem.* **1992**, *31*, 5193.
(34) Sheldrick, G. M. In *Crystallographic Computing*; Sheldrick, G. M., Krüger, C., Goddard, R., Eds.; Oxford University Press: Oxford, 1985; p 175.
(35) Sheldrick, G. M. *SHELXTL-PC Version 4.1*; Siemens Analytical X-ray Instruments, Inc.: Madison, WI, 1989.

Table 1. Experimental Details of the X-ray Diffraction Studies[a] of $[Fe_{16}MnO_{10}(OH)_{10}(O_2CPh)_{20}]\cdot 3MeCN\cdot 2Et_2O$ (**1**·3MeCN·2Et$_2$O), $[Fe_{17}O_{10}(OH)_{10}(O_2CPh)_{20}]\cdot 18MeCN$ (**2**·18 MeCN), and $[Fe_{16}CoO_{10}(OH)_{10}(O_2CPh)_{20}]\cdot 17MeCN$ (**3**·17MeCN)

	1·3MeCN·2Et$_2$O	**2**·18MeCN	**3**·17MeCN
formula	$C_{154}H_{139}Fe_{16}MnN_3O_{62}$	$C_{176}H_{164}Fe_{17}N_{18}O_{60}$	$C_{174}H_{161}CoFe_{16}N_{17}O_{60}$
formula weight, g mol^{-1}	3972.27	4440.72	4402.75
crystal system	triclinic	triclinic	triclinic
space group	$P\bar{1}$	$P\bar{1}$	$P\bar{1}$
a, Å	17.447(5)	16.781(2)	16.9237(9)
b, Å	19.143(4)	17.316(2)	17.531(1)
c, Å	14.720(3)	18.044(2)	18.144(1)
α, deg	106.96(2)	105.075(9)	105.365(5)
b, deg	95.24(2)	99.997(7)	99.501(4)
γ, deg	65.22(2)	104.209(9)	104.704(5)
V, Å^3	4267(4)	4747.5(9)	4862(1)
Z	1	1	1
T, °C	−75	−90	23
ρ_{calcd}, g cm^{-1}	1.546	1.555	1.503
crystal dimensions, mm^3	0.25 × 0.23 × 0.20	0.26 × 0.28 × 0.50	0.30 × 0.20 × 0.13
transmission factor range	0.713–1.000	0.807–1.000	0.923–1.000
crystal decay	0.5%	0.0%	0.0%
linear abs coeff, cm^{-1}	14.7	13.2	13.2
data collected	$3° \le 2\theta \le 45$; $\pm h, \pm k, +l$	$3° \le 2\theta \le 47.5$; $+h, \pm k, \pm l$	$2° \le 2\theta \le 50$; $+h, \pm k, \pm l$
reflections collected	11805	15160	18276
R_{avg} for refl averaging	0.043	0.022	0.038
no. of independent data	11 115	14 453	17 080
no. of unique data with $I > 3\sigma(I)$	6627	10 248	7603
no. of variables	698	1212	795
$F(0,0,0)$	2021	2268	2247
R^b	0.077	0.043	0.060
R_w^c	0.103	0.040	0.080

[a] Data collected on an Enraf–Nonius CAD4-F kappa geometry diffractometer with graphite-monochromatized Mo K$\bar{\alpha}$ radiation ($\bar{\lambda}$ = 0.71073 Å). [b] $R = \sum||F_o| - |F_c||/\sum|F_o|$. [c] $R_w = [\sum w(|F_o| - |F_c|)^2/\sum w|F_o|^2]^{1/2}$, where $w = 4F^2/\sigma^2(F^2)$ and $\sigma^2(F^2) = [S^2(C + 4B) + (pI)^2]/(Lp)^2$, with S = scan rate, C = peak counts, B = sum of left and right background counts, I = reflection intensity, Lp = Lorentz-polarization factor, and p is a constant employed to avoid overweighting of intense reflections.

Table 2. Summary of Bond Distances for $[Fe_{16}MnO_{10}(OH)_{10}(O_2CPh)_{20}]\cdot 3MeCN\cdot 2Et_2O$ (**1**·3MeCN·2Et$_2$O), $[Fe_{17}O_{10}(OH)_{10}(O_2CPh)_{20}]\cdot 18MeCN$(**2**·18MeCN) and $[Fe_{16}CoO_{10}(OH)_{10}(O_2CPh)_{20}]\cdot 17MeCN$ (**3**·17MeCN)

type of bond	range for **1** [mean][a]	range for **2** [mean][a]	range for **3** [mean][a]
Mn(Fe,Co)—$O_{\mu 4\text{-oxo}}$	2.021(7)–2.033(10) [2.028(5)]	2.021(3)–2.055(3) [2.03(2)]	2.029(7)–2.056(8) [2.04(1)]
Fe—$O_{\mu 4\text{-oxo}}$	1.954(7)–2.121(9) [2.04(6)]	1.887(3)–2.090(3) [2.01(7)]	1.955(7)–2.087(5) [2.03(4)]
Fe—$O_{\mu 3\text{-oxo}}$	1.892(7)–2.058(10) [1.95(6)]	1.894(3)–1.957(3) [1.92(4)]	1.901(5)–1.958(7) [1.92(2)]
Fe—$O_{\mu 3\text{-hydroxo}}$	2.018(12)–2.311(10) [2.11(8)][b]	1.999(3)–2.311(4) [2.11(8)][c]	2.009(7)–2.359(9) [2.11(9)][d]
Fe—$O_{\mu 2\text{-hydroxo}}$	1.922(7)–1.944(8) [1.93(1)]	1.923(4)–1.956(3) [1.94(2)]	1.924(7)–1.947(7) [1.94(1)]
Fe—$O_{benzoate}$	1.966(9)–2.136(12) [2.03(4)]	1.971(4)–2.133(4) [2.03(4)]	1.972(8)–2.139(8) [2.02(4)]
C—$O_{benzoate}$	1.221(13)–1.290(14) [1.26(2)]	1.208(6)–1.284(6) [1.26(2)]	1.238(15)–1.282(11) [1.26(1)]

[a] Numbers in parentheses are estimated standard deviations in the last significant digit or, in the case of mean values, the standard deviation of the mean given by $s = [\sum(x^2 - \bar{x}^2)/(n-1)]^{1/2}$. [b] If the extreme value of 2.311(10) Å is neglected, the maximum is 2.179(10) Å and the mean is 2.09(5) Å. [c] If the extreme value of 2.311(4) Å is neglected, the maximum is 2.212(4) Å and the mean is 2.08(6) Å. [d] If the extreme value of 2.359(9) Å is neglected, the maximum is 2.124(7) Å and the mean is 2.08(4).

non-hydrogen atoms were refined anisotropically; hydrogen atoms were included as reported for **1**·2Et$_2$O·3MeCN. Final refined positional and thermal parameters and full lists of bond distances and angles may be found in Tables S4–S6, respectively. Selected bond distances are included in Table 2.

The structure of **3**·17MeCN was solved in space group $P\bar{1}$ by using the direct methods option of SHELXS-86,[34] which revealed most of the structure. The remaining non-hydrogen atoms were located from difference Fourier maps, and the structure was refined by least-squares techniques with SHELXTL-PC.[35] The asymmetric unit contains a total of 8.5 molecules of acetonitrile; six have been refined with single occupancy, one with half-occupancy, and two with a single acetonitrile molecule disordered over two overlapping sites. The geometry of these groups has been fixed close to linear with bond lengths set to the mean of the full occupancy molecules. Anisotropic thermal parameters were assigned to all the non-hydrogen atoms except those of the phenyl rings and solvent molecules. Hydrogen atoms were inserted as described for **1**·2Et$_2$O·3MeCN, except for those of the disordered acetonitrile molecules, which were not included. Final refined positional and thermal parameters and full lists of bond distances and angles may be found in Tables S7–S9, respectively. Selected bond distances are included in Table 2.

Magnetic Susceptibility Measurements. Variable-temperature solid-state magnetic susceptibility measurements were carried out on vacuum-dried samples of **1** (70.5 mg) and **2** (34.6 mg) at 5 kOe at temperatures ranging from 2.65 to 323 K for **1** and 2.10 to 300 K for **2** with an SHE Model 905 SQUID-type susceptometer. The dependence of the magnetization was also measured at several temperatures for **1** and **2** to ensure that the fields selected for the variable-temperature studies were within the linear, presaturation regime of the magnetization versus H/T curves for the two compounds. The sample of **1** was measured in a Kel-F polymer sample holder, and the small contribution of the sample holder to the total susceptibility was ignored. Compound **2** was measured in a Si–Al alloy sample holder, the susceptibility of which was measured at all of the temperatures and fields employed to allow for accurate correction of the paramagnetic contribution of the sample holder to the total susceptibility.

High-Field Magnetization Studies. Studies of the field dependence of the magnetization for **1** (70.5 mg) and **2** (26.0 mg) were carried out at fields ranging from 0 to 197 and 0 to 191 kOe, respectively. Samples were measured in Kel-F sample holders by using a vibrating sample magnetometer (VSM)[37] suspended in the bore of a water-cooled, Bitter electromagnet. The negligible diamagnetic contribution of the Kel-F sample holders to the total measured moment was ignored in the workup of the data.

Mössbauer Spectroscopy. Mössbauer spectra of polycrystalline samples of **1** and **2** were collected at temperatures ranging from 1.8 to 80 and 2.0 to 20 K, respectively, and fields ranging from 0 to 80 kOe, by using a

(36) *TeXsan: Single Crystal Structure Analysis Software, Version 1.6c*; Molecular Structure Corp.: The Woodlands, TX, 1994.

(37) Foner, S., Jr.; McNiff, E. J., Jr. *Rev. Sci. Instrum.* **1968**, *39*, 171.

conventional, constant acceleration spectrometer equipped with a superconducting magnet. The applied magnetic field was parallel to the γ-ray propagation direction. The source was ^{57}Co in a Rh matrix. Isomer shifts were referenced to iron metal at 300 K. The spectra were least-squares fit assuming a distribution of internal hyperfine fields.

Results and Discussion

Synthesis and Spectral Properties. Compounds of general formula $[Fe_{16}MO_{10}(OH)_{10}(O_2CPh)_{20}]$, M = Mn (**1**), Fe (**2**), or Co (**3**), were prepared in low to modest yields by crystallization from acetonitrile/water solutions containing the appropriate divalent metal ion and $\{Fe_3O\}^{7+}$ or, in the case of **2**, $\{Fe_3O\}^{6+}$. A major product obtained from each of these reactions is $\{Fe_{11}\}$, which was identified by comparison of its infrared spectrum and unit cell parameters with published values.[26] Although the infrared spectra of **1**–**3** and $\{Fe_{11}\}$ are rather similar above 1000 cm^{-1}, there are distinguishing features ~560–700 cm^{-1} which allow the two classes of compound to be identified (Figures S1–S4, supplementary material). In particular, the $\{Fe_{16}M\}$ complexes can be identified by the presence of three weak to medium intensity bands in the range 812–844 cm^{-1}. The $\{Fe_3O\}^{n+}$ complexes have only two bands in this region, and for $\{Fe_{11}\}$ there is a relatively strong absorption at 809 cm^{-1}. In addition, the $\{Fe_{16}M\}$ complexes show two ν_s(OH) stretches in the 3595–3559-cm^{-1} region.

If M^{2+} is replaced by Fe(III) in the synthesis and the drying step is omitted, $\{Fe_{11}\}$ is obtained as the only product in 58% yield after 10 days. When the preparation of **2** was attempted by the same route as used in the synthesis of **1**, but under anaerobic conditions, the mixed-valence triangular cluster $[Fe_3O(O_2CPh)_6(H_2O)_2(MeCN)]\cdot MeCN$ was obtained in 8.4% yield. This complex was identified by infrared spectroscopy, elemental analysis, and X-ray crystallography.[38] Omission of the reflux and drying steps in the preparation of **1** led to formation of very dark brown microcrystals of the mixed-metal, mixed-valence complex $[Fe_2MnO(O_2CPh)_6(H_2O)_3]$. This product was identified from its infrared spectrum, which is identical to that of the mixed-valence iron complex, and by elemental analysis.[39] Efforts were made to isolate **3** from an intimate mixture of the desired product and $\{Fe11\}$. Addition of *o*-dichlorobenzene produced an orange-red solution and a small amount of insoluble brown microcrystals after several days. Elemental analysis identified the brown product as $[Fe_2CoO(O_2CPh)_6(H_2O)_3]\cdot 2H_2O$.[40]

These observations illustrate the lability of the $\{Fe_3O\}^{n+}$ starting materials in solution. The mixed valence complex $\{Fe_3O\}^{6+}$ was more effective than $\{Fe_3O\}^{7+}$ in the preparation of complex **2**, suggesting that this species might be an intermediate in the formation of $\{Fe_{16}M\}$. This hypothesis is supported by the appearance of a very dark brown color as soon as the Mn(II) ion is added in the preparation of **1**, reminiscent of the appearance of $\{Fe_2Mn\}^{6+}$.

The $\{Fe_{16}M\}$ complexes are insoluble in most solvents, but will dissolve in hot acetonitrile or pyridine. It seems unlikely, however, that the heptadecanuclear complex remains intact in solution. The EPR spectrum of a frozen (45 K) solution of **1** in pyridine revealed a six-line pattern typical of those observed for mononuclear Mn(II) (g = 2.00, $A = 8.9 \times 10^{-3}$ cm^{-1}). Integration of the signal showed that it accounted for all of the manganese in the sample. Since weak magnetic coupling generally results in loss of the six hyperfine lines, the most likely explanation for these observations is that the complex is no longer assembled and that the manganese is present as a mononuclear species. Because the crystal structures of **2** and **3** are isomorphous, we considered the possibility that they were both Fe_{17} species. The presence of Co in **3** was verified by EPR spectroscopy, however. A solid-state spectrum recorded at 12 K displayed an axial signal at g = 4.4, a value characteristic of high-spin octahedral Co(II).[41–43]

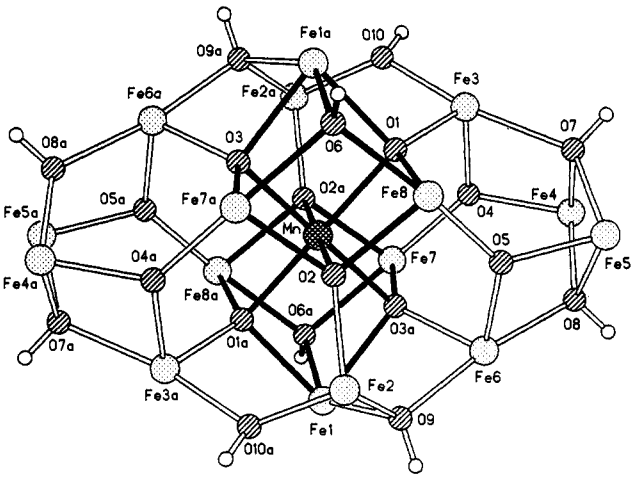

Figure 2. Perspective view of the metal atoms and the μ-oxo and μ-hydroxo ligands of the core of **1**. Atoms are shown as spheres of arbitrary radius for clarity. The $[Fe_3O_3(OH)_2]_2M$ double cube is highlighted.

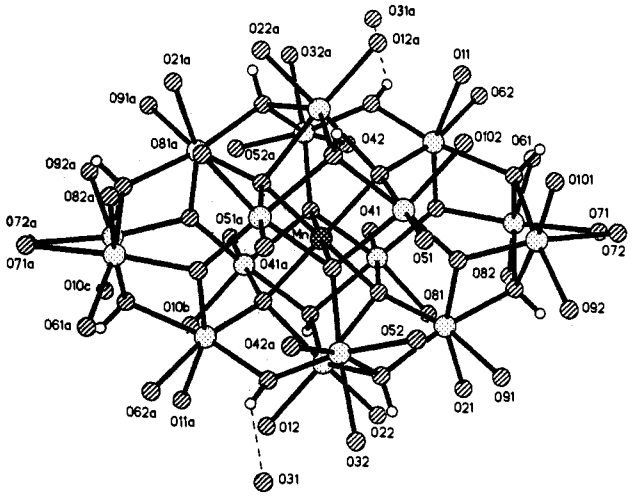

Figure 3. Perspective view of the metal atoms, μ-oxo and μ-hydroxo ligands, and coordinated benzoate oxygen atoms in **1**. Atoms are shown as spheres of arbitrary radius for clarity. Labels have been omitted for the metals and the μ-oxo and μ-hydroxo for clarity.

Description of the Structures. The structure of **3** has been described briefly previously.[30] Compounds **1**, **2**, and **3** have nearly identical geometries, features of which are depicted in Figures 2–4 for the $\{Fe_{16}Mn\}$ compound. Selected bond lengths and angles are given in Table 2. All three compounds have a crystallographically imposed inversion center. Since divalent Mn, Fe, or Co is the unique atom in the molecular formula, it was assigned to this site. There is no evidence of a Jahn–Teller distortion at the manganese atom in **1**, consistent with the central ion remaining in the divalent state. This heteroatom (M) forms the shared corner of an $\{[Fe_3O_3(OH)]_2M\}$ double cube (Figure 2). Whereas structures containing iron–chalcogen cubes are well-known for sulfur,[44–46] selenium,[47] and tellurium,[48] no previous examples of

(38) $[Fe_3O(O_2CPh)_6(H_2O)_{2.5}(MeCN)_{0.5}]MeCN$: Anal. ($C_{43}H_{36.5}O_{15.5}N_{0.5}Fe_3$) Found (Calcd) C, 53.45 (53.15); H, 3.66 (3.91); IR (inter alia) 1600, 1563, 1545, 1402, 1177, 1026, 839, 817, 720, 689, 674, 618, 593 cm^{-1}. Crystal data: triclinic, a = 12.604(2) Å, b = 13.994(5) Å, c = 15.549(6) Å, α = 116.44(3)°, β = 106.40(2)°, γ = 98.88(5)°, V = 2227(1) Å^3, space group P$\bar{1}$, R = 0.081.

(39) $[Fe_2MnO(O_2CPh)_6(H_2O)_3]$: Anal. ($C_{42}H_{36}O_{16}Fe_2Mn$) Found (Calcd) C, 51.77 (52.36); H, 3.61 (3.76); Fe, 11.52 (11.59); IR (inter alia) 1601, 1563, 1546, 1401, 1177, 1025, 839, 818, 720, 689, 673, 590, 543, 460 cm^{-1}.

(40) $[Fe_2CoO(O_2CPh)_6(H_2O)_3]\cdot 2H_2O$: Anal. ($C_{42}H_{40}O_{18}CoFe_2$) Found (Calcd) C, 50.83 (50.28); H, 3.93 (4.02); Co, 6.10 (5.87); Fe, 10.23 (11.13).

(41) Carlin, R. L. In *Transition Metal Chemistry*; Carlin, R. L., Ed.; Marcel Dekker, Inc.: New York, 1965; Vol. 1.

(42) Mizuno, K.; Lunsford, J. H. *Inorg. Chem.* **1983**, *22*, 3484.

(43) Migita, K.; Chikira, M.; Iwaizumi, M. *J. Chem. Soc., Dalton Trans.* **1983**, 2281.

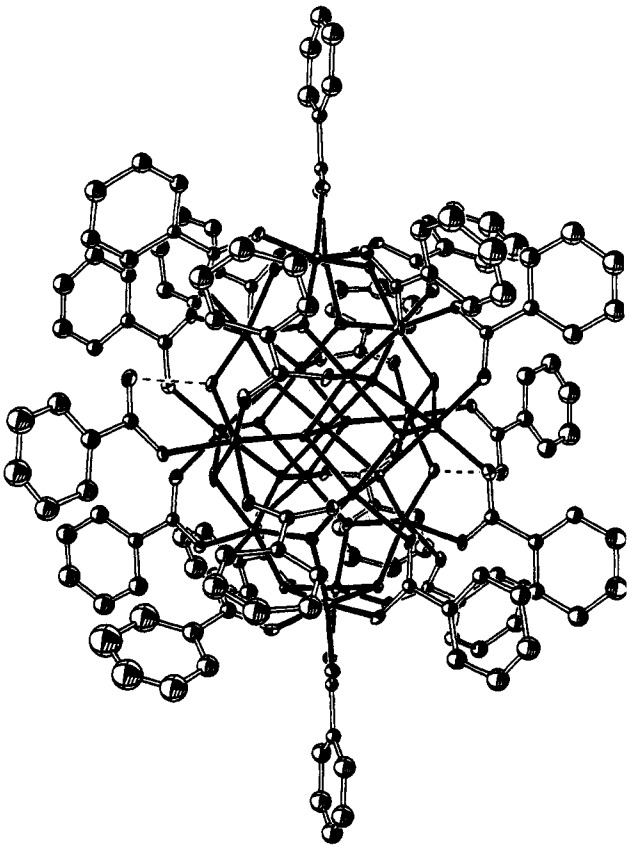

Figure 4. Thermal ellipsoid plot (40% probability) showing an entire molecule of **1**. Labels have been omitted for clarity. Metal—oxygen bonds are shown as filled lines, whereas C—O and C—C are depicted as open lines. Dashed lines represent hydrogen bonds.

an iron–oxo–hydroxo cube were known prior to the preliminary report of the structures of **1** and **3**.[30] Subsequently, several molecules containing such units have been synthesized.[27,49] In contrast, numerous manganese–oxygen cubes have been characterized recently.[49-54] The double cube is surrounded by an $[Fe_{10}O_4(OH)_8]$ cage (Figure 3), which, in turn, is encapsulated within a shell of 20 benzoate ligands (Figure 4). All the metal atoms are six-coordinate, although there is one unusually long bond (Fe1—O9, 2.31(1), 2.311(4), and 2.359(9) Å for **1**, **2**, and **3**, respectively) and one short nonbonding interaction (Fe1—O10, 2.96(1), 2.874(4), and 2.99(1) Å for **1**, **2**, and **3**, respectively). All the donor atoms are oxygen, contributed from either oxo, hydroxo, or benzoate groups. The central metal atom is unique

(44) Berg, J. M.; Holm, R. H. In *Iron-Sulfur Proteins*; Spiro, T. G., Ed.; Wiley-Interscience: New York, 1982; p 1.
(45) Münck, E.; Papaefthymiou, V.; Surerus, K. K.; Girerd, J.-J. In *Metal Clusters in Proteins*; Que, L., Jr., Ed.; ACS Symposium Series 372; American Chemical Society: Washington, DC, 1988; p 302.
(46) Averill, B. A. In *Metal Clusters in Proteins*; Que, L., Jr., Ed.; ACS Symposium Series 372; American Chemical Society: Washington, DC, 1988; p 258.
(47) Bobrik, M. A.; Laskowski, E. J.; Johnson, R. W.; Gillum, W. O.; Berg, J. M.; Hodgson, K. O.; Holm, R. H. *Inorg. Chem.* **1978**, *17*, 1402.
(48) Simon, W.; Wilk, A.; Krebs, B.; Henkel, G. *Angew. Chem., Int. Ed. Engl.* **1987**, *26*, 1009.
(49) Taft, K. L.; Caneschi, A.; Pence, L. E.; Delfs, C. D.; Papaefthymiou, G. C.; Lippard, S. J. *J. Am. Chem. Soc.* **1993**, *115*, 11753.
(50) McKee, V.; Shepard, W. B. *J. Chem. Soc., Chem. Commun.* **1985**, 158.
(51) Brooker, S.; McKee, V.; Shepard, W. B.; Pannell, L. K. *J. Chem. Soc., Dalton Trans.* **1987**, 2555.
(52) Kulawiec, R. J.; Crabtree, R. H.; Brudvig, G. W.; Schulte, G. K. *Inorg. Chem.* **1988**, *27*, 1309.
(53) Li, Q.; Vincent, J. B.; Libby, E.; Chang, H.-R.; Huffman, J. C.; Boyd, P. D. W.; Christou, G.; Hendrickson, D. N. *Angew. Chem., Int. Ed. Engl.* **1988**, *27*, 1731.
(54) Boyd, P. D. W.; Li, Q.; Vincent, J. B.; Folting, K.; Chang, H.-R.; Streib, W. E.; Huffman, J. C.; Christou, G.; Hendrickson, D. N. *J. Am. Chem. Soc.* **1988**, *110*, 8537.

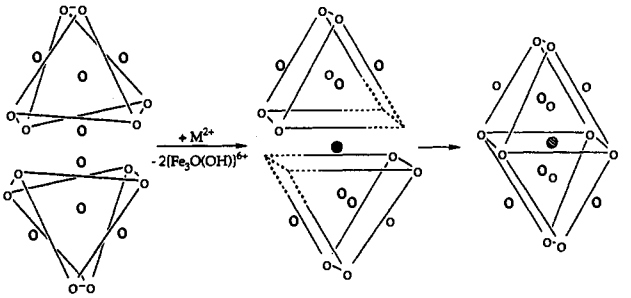

Figure 5. Depiction of the formation of $\{Fe_{16}M\}$ from two $\{Fe_{11}\}$ units, where iron atoms are shown as open circles and the M atom as a shaded circle.

in that it is bonded only to oxo donors; the 16 iron atoms all have coordination spheres containing each type of ligand in various ratios. The geometry about the metal ions varies from nearly octahedral, for Mn, Fe9, or Co, to severely distorted for Fe1 (angular values of 70.2(4)–113.5(4)°, 71.3(1)–115.9(1)°, and 70.7(3)–112.0(3)° for **1**, **2**, and **3**, respectively) or Fe6 (79.9(4)–106.3(4)°, 79.5(1)–104.1(6)°, and 80.3(3)–105.5(3)° for **1**, **2**, and **3**, respectively). Similar distortions were previously observed in the related (vide infra) structure of $[Fe_{11}O_6(OH)_6(OCPh)_{15}]$.[26] The distances between adjacent metal atoms vary over quite a wide range, from 2.947(2) (2.9411(8), 2.951(2)) Å for Mn—Fe8 (Fe9—Fe8 and Co—Fe8) to 3.670(2) (3.6774(8), 3.692(2)) Å for Mn—Fe2 in **1** (Fe9—Fe2 in **2** and Co—Fe2 in **3**). The shortest metal–metal distances are between metals that are linked by two oxo bridges, whereas the longest are for pairs of metal ions with only a single atom bridge between them.

Stoichiometry requires that the oxygen atoms of the $[Fe_{16}MO_{10}(OH)_{10}]$ core are comprised of 10 oxo and 10 hydroxo ligands. The five crystallographically independent oxo and hydroxo groups can be assigned on the basis of their coordination properties. Atoms O1, O2, and O3 are coordinated approximately tetrahedrally to four metal ions and can therefore be designated oxo groups. Both O4 and O5 are coordinated to three metal atoms with approximately planar geometries, the angle sums about these respective oxygen atoms for **1** (**2** and **3**) being 356.6° (355.3° and 357.5°) and 357.9° (356.8° and 357.8°), respectively, and are therefore also likely to be oxo groups. Atoms O6, O7, O8, and O9 are bonded to three iron atoms with pyramidal geometry (angle sums 296.7° (297.8°, 295.9°), 320.1° (321.9°, 321.4°), 318.0° (319.9°, 320.7°), and 326.9° (324.7°, 325.2°) for O6, O7, O8, and O9, respectively), suggesting that these are hydroxo donors. Further evidence for this identification is provided by the hydrogen bonds from O6, O7, and O8 to lattice solvent (average bond distances are 2.92(3), 2.94(1), and 2.94(9) Å for **1**, **2**, and **3**, respectively). All hydrogen bonds are to acetonitrile nitrogens except for O6 in compound **1**, which is interacting with the oxygen of interstitial diethyl ether. The final oxygen atom (O10) is coordinated to only two iron atoms. It can be identified as hydroxide from stoichiometry and because it is involved in hydrogen bonding with the acceptor oxygen atom of a terminal benzoate group.

Nine of the 10 independent benzoate ligands are bidentate and bridge two iron atoms (Figure 4). The exception is a monodentate ligand coordinated to Fe2; the second benzoate oxygen atom of this residue is hydrogen bonded to a coordinated hydroxide (O10—O31, 2.68(1), 2.690(5), and 2.69(1) Å for **1**, **2**, and **3**, respectively).

Formal Construction of the Clusters. Although the mechanism by which clusters **1**–**3** are assembled has not been established, they may formally be constructed by fusion of two molecules of $[Fe_{11}O_6(OH)_6(O_2CPh)_{15}]$. In this procedure, illustrated in Figure 5, each twisted, pentacapped trigonal prism of $\{Fe_{11}\}$ loses one $\{Fe_3O(OH)(O_2CPh)_5\}^+$ fragment, similar to those present in basic

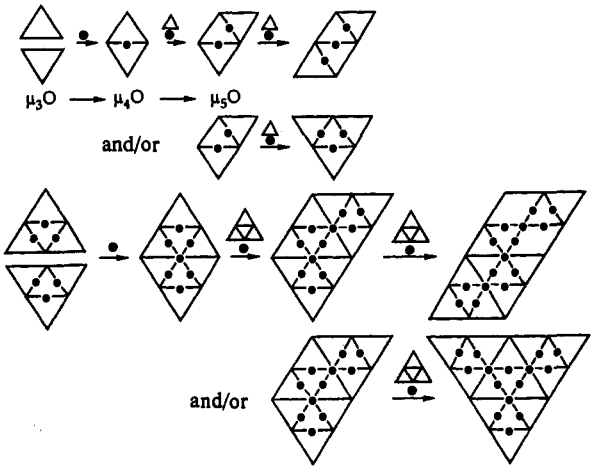

Figure 6. Depiction of the formation of larger clusters from $\{Fe_{11}\}$ units. The $\{Fe_{11}\}$ units are given as triangles and M as filled circles.

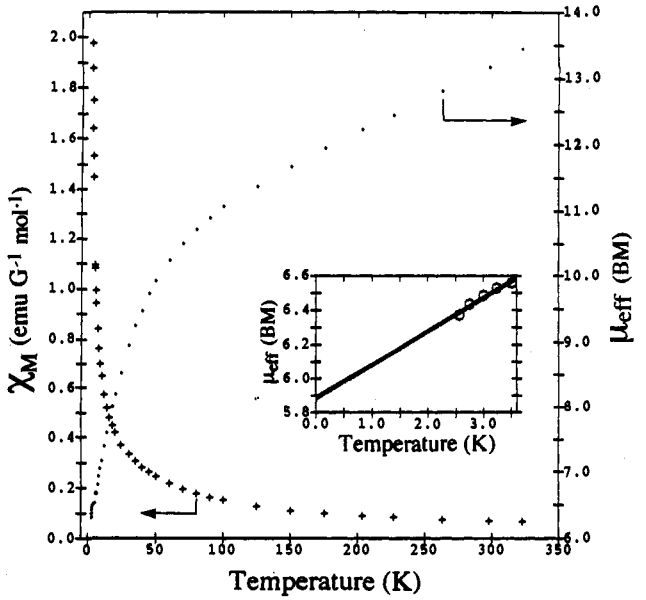

Figure 7. Temperature-dependent molar susceptibility (+) and effective moment (•) plot for **1** at 5 kOe. The inset depicts a least-squares extrapolation of the effective moment for **1** to 0 K for ground-state estimation (see text).

iron carboxylates.[55] The remaining $\{Fe_8O_5(OH)_5(O_2CPh)_{10}\}^-$ fragments then combine about a divalent M^{2+} ion, forming an octacapped, body-centered octahedron (Figure 5). The same procedure can, in theory, be repeated to form larger clusters, as indicated in Figure 6. These larger aggregates are predicted to have the general formula $M_nFe_{5n+11}O_{4n+6}(OH)_{4n+6}(O_2CPh)_{5n+15}$, where $n = 1, 2, 3$, etc. A related possibility is that the $\{Fe_8\}$ units are intermediates in the formation of $\{Fe_{11}\}$ and $\{Fe_{16}M\}$.

Magnetic Properties of 1 and 2. Variable-temperature molar magnetic susceptibility (χ_M) studies reveal that χ_M increases with decreasing temperature for both **1** and **2** (Figures 7 and 8, respectively). Calculation of the effective moments (μ_{eff}) from susceptibilities indicates that the μ_{eff} decreases from 13.22 μ_B per molecule (3.21 μ_B per metal) at 298 K to 6.36 μ_B per molecule (1.54 μ_B per metal) at 2.56 K for **1** (Figure 7). A similar decrease in the μ_{eff} from 13.33 μ_B per molecule (3.23 μ_B per metal) at 300 K to 6.44 μ_B per molecule (1.56 μ_B per metal) at 2.0 K is observed for **2** (Figure 8). This result demonstrates that the metal centers are coupled antiferromagnetically. The theoretical minimum

(55) Cannon, R. D.; White, R. P. *Prog. Inorg. Chem.* **1988**, *36*, 195 and references therein.

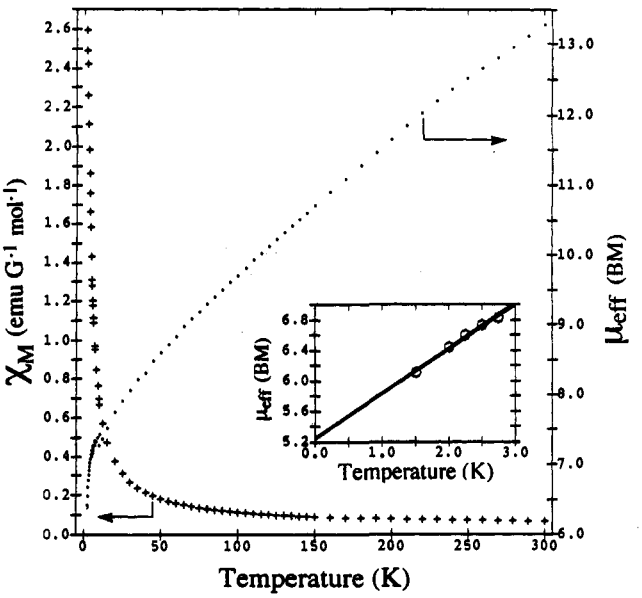

Figure 8. Temperature-dependent molar susceptibility (+) and effective moment (•) plot for **2** at 5 kOe. Shown in the inset is a least-squares extrapolation of the effective moment to 0 K for ground-state estimation (see text).

spin state is $S = 1/2$ for **1**. That is, at the most, 84 of the 85 d electrons in **1** can be spin paired, leaving the odd electron unpaired. The maximum spin state would be $S = 85/2$, corresponding to the spin alignment of all 85 of the d electrons in the system. On the other hand, a molecule of **2** is an even electron system, with 16 $S = 5/2$ ferric ions and one $S = 2$ ferrous ion, giving a total of 84 d electrons, which can all spin couple through superexchange interactions to give a minimum spin state of $S = 0$ and maximum spin of $S = 84/2$. An attempt to estimate the total ground spin state S_T, for both **1** and **2** was made on the basis of an extrapolation of the μ_{eff} to 0 K from the lowest temperature portion of the μ_{eff} versus temperature curves. This approach neglects possible complexity arising from zero-field splitting contributions. Since there is no isolated ground spin state in these complex molecules (vide infra), however, it is not possible to make an accurate estimate of zero-field splitting effects. For **1** the extrapolated value of μ_{eff} at 0 K is ~5.9 μ_B (Figure 7, inset). This value corresponds closely to that of $\mu_{eff} = 5.91$ μ_B calculated from the spin-only equation for effective moment (eq 1) for a total spin

$$\mu_{eff} = [g^2 S_T(S_T + 1)]^{1/2} \quad (1)$$

of $S_T = 5/2$ and $g = 2.00$. This S_T value corrects a previous report of $S_T \leq 1$ for **1**.[30] The sample measured earlier was subsequently found by a low-temperature Mössbauer study to have been contaminated with a diamagnetic impurity.[56] Extrapolation of the low-temperature μ_{eff} plot for **2**, including a 1.5 K point from high-field magnetization studies, gave a value of ~5.3 μ_B at 0 K (Figure 8, inset). This value approaches that of 4.90 μ_B calculated from eq 1 for a spin of $S_T = 2$ and a $g = 2.00$.

The slope of the μ_{eff} versus temperature curve for **1** decreases smoothly up to ~100 K, after which it stabilizes at ~0.01 μ_B/K, giving rise to a linear increase in μ_{eff} up to 322 K. The μ_{eff} of **2** rises very rapidly between 2 and 3 K, with a slope >0.5 μ_B/K. Between 3 and 40 K, the slope decreases to ~0.2 μ_B/K, where it remains between 40 and 300 K, giving rise to a roughly linear

(56) Papaefthymiou, G. C.; Rardin, R. L.; Lippard, S. J. Unpublished results. The current measurements were made on a pure sample, as judged by elemental analysis and Mössbauer spectroscopy, and yielded higher values for the magnetic moment and susceptibility over the entire temperature range measured than those for the previously measured sample.

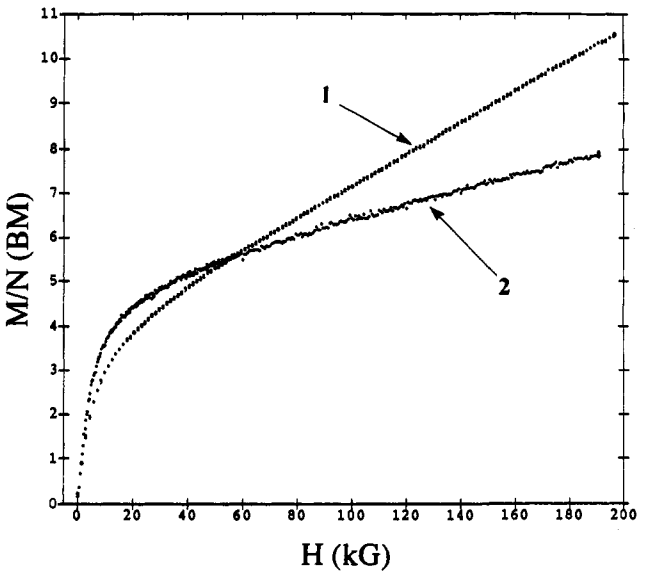

Figure 9. Results of high-field magnetization studies of **1** at 1.48 K and **2** at 1.50 K. The reduced magnetic moment is plotted versus the applied field strength.

region in the higher temperature regime. The μ_{eff} values for both **1** and **2** continue to increase, even at 300 K. Neither **1** nor **2** reaches saturation in μ_{eff}, even at room temperature, indicative of the presence of a band-like,[57] high density of electronic states that are becoming thermally accessible. Although the μ_{eff} versus temperature curves for **1** and **2** are similar at the lower and higher temperatures, their shapes are significantly different.

The lack of saturation in the μ_{eff} versus T curves is also reflected in the absence of saturation in the magnetization versus applied magnetic field curves shown in Figure 9 for fields up to 200 kOe, taken at the high-field facility of the Francis Bitter National Magnet Laboratory. The magnetization increases monotonically without saturating as the field increases for both compounds. This feature is also present in magnetization curves of ferritin at 20 K and up to 15 kOe applied field[58] and of freeze-dried ferritin at 77 K up to 200 kOe.[59] No hysteresis in the magnetization and no remnant moment were observed when the field was swept to the maximum value and back to 0 kOe for either compound. The maximum values of the reduced magnetic moments for **1** and **2** were 10.6 and 8.0 μ_B, respectively, intermediate between the magnetization values expected for the extrapolated ground states and the full magnetization values of the aggregates (all of the spins aligned). For **1**, the maximum magnetization observed represents 12% of the full magnetization of the cluster, 85 μ_B, calculated from eq 1. The maximum magnetization obtained for **2** represents only 9% of the possible maximum of 84 μ_B.

Mössbauer Spectroscopy. Both complexes **1** and **2** exhibit paramagnetic Mössbauer spectra consisting of symmetric quadrupole doublets down to *ca.* 10 K (Figures S5 and S6). Complex **1** has $\delta = 0.51$ mm s^{-1} and $\Delta E_Q = 0.77$ mm s^{-1} at 80 K,[13] whereas for **2** $\delta = 0.48$ mm s^{-1} and $\Delta E_Q = 0.82$ mm s^{-1} at 20 K[31,60] relative to metallic iron at room temperature. The isomer shifts are comparable to those of oxo-bridged high-spin ferric complexes,[61] but the quadrupole splittings are smaller than those observed[62,63] for oxo-bridged complexes (1.5–2.0 mm s^{-1}) and approach those reported for polyiron oxo and hydroxo compounds such as Fe_2O_3, FeOOH, and the iron core of ferritin.[64] No distinct signal due to a ferrous ion was observed for **2**, indicating electronic delocalization within the cluster.[60] If the observed absorption were due only to 16 Fe(III) ions, an additional doublet arising from localized Fe(II) would be expected. Given the excellent statistics of the spectrum, the high-velocity absorption line of such a doublet should have easily been detected. Its absence suggests delocalization of the extra d electron contributed to the cluster by the ferrous center.

At low temperatures both complexes exhibit relaxation phenomena similar to those of superparamagnets. In both **1** and **2**, magnetic hyperfine lines appear below 6 K, superimposed on a broad absorption envelope at the center of the spectrum. With decreasing temperature the intensity of the magnetic subspectrum increases at the expense of the central doublet. The position of the outer magnetic lines does not shift over the transitional temperature range, behavior similar to that of small particle superparamagnets. In the $\{Fe_{16}M\}$ molecules, the benzoate shell surrounding each cluster keeps the magnetic cores isolated from one another. Crystal packing diagrams indicate a distance between cluster centroids of ~20 Å over which dipole–dipole magnetic interactions are negligible.[65] Thus, the magnetic, in conjunction with the applied field (vide infra), spectra manifest short-range intracluster magnetic order, indicating that these systems straddle the molecular/solid-state boundary. The estimated effective blocking temperature, the temperature at which the absorption area under the magnetic subspectrum equals that of the central doublet, is $T_B' \approx 4$ K and ≈ 2 K for **1** and **2**, respectively.[31] Since the sizes of the two clusters are identical, the difference in thermal spectral behavior indicates a smaller anisotropy constant for **2** than for **1**.[31]

Figures S7–S8 show spectral behavior in the presence of an external magnetic field, $H_a = 60$ kOe, applied parallel to the direction of the 14.4-keV γ-rays; spectra in zero field are also shown for comparison. Whereas at 4.2 K in zero field both compounds **1** and **2** exhibit a strong absorption doublet at the center of the spectrum (Figures S5–S6), at the same temperature upon application of the field only magnetically split spectra are observed (Figures S7–S8). The six lines in each spectrum correspond to the two $\Delta m = 0$ (lines 2 and 5) and the four $\Delta m = \pm 1$ lines of a magnetic hyperfine spectrum.[61] It is most notable that (a) upon application of the external field the middle $\Delta m = 0$ absorption lines persist and (b) the overall magnetic splitting, which is a measure of the internal magnetic field at the iron nucleus, does not change significantly upon application of the field. These observations reveal deviation from simple paramagnetic Mössbauer behavior commonly observed in iron clusters.[66] More extensive discussion of these phenomena may be found elsewhere.[13,60]

The temperature dependence of the Mössbauer spectral features of **1** and **2** prompted us to investigate whether their magnetization versus H/T curves superimpose for different values of T, behavior often used as the operational definition of classical superparamagnetism.[67] In particular, theoretical studies of superpara-

(57) With increasing cluster size the discrete energy levels of molecular systems give rise to electronic energy levels grouped together in a band-like structure encountered in extended systems. See for example: You, J.-F.; Snyder, B. S.; Papaefthymiou, G. C.; Holm, R. H. *J. Am. Chem. Soc.* **1990**, *112*, 1067. You, J.-F., Papaefthymiou, G. C.; Holm, R. H. *J. Am Chem. Soc.* **1992**, *114*, 2697.

(58) Blaise, A.; Chappert, J.; Girardet, J.-L. *C. R. Hebd. Seances Acad. Sci.* **1965**, *261*, 2310.

(59) Frankel, R. B.; Papaefthymiou, G. C.; Watt, G. To be submitted for publication.

(60) Papaefthymiou, G. C. In *Clusters and Cluster Assembled Materials*; Averbach, R. S., Bernholc, J., Nelson, D. L., Eds.; MRS Symposium Proceedings; Materials Research Society: Pittsburgh, PA, Vol. 206, 1991; p 539.

(61) Greenwood, N. N.; Gibb, T. C. *Mössbauer Spectroscopy*; Chapman and Hall, Ltd.: London, 1971.

(62) Kurtz, D. M., Jr. *Chem. Rev.* **1990**, *90*, 585.

(63) Murray, K. S. *Coord. Chem. Rev.* **1974**, *12*, 1.

(64) Watt, G. D.; Frankel, R. B.; Papaefthymiou, G. C. *Proc. Natl. Acad. Sci. U.S.A.* **1985**, *82*, 3640.

(65) The dipole–dipole interaction energy, $\vec{\mu}\cdot\vec{\mu}/r^3$, is on the order of 10^{-20} ergs for dipoles separated by a distance of 20 Å. This value is much weaker than the thermal energy, kT, for the lowest temperature employed, which is on the order of 10^{-16} ergs.

(66) Girerd, J.-J.; Papaefthymiou, G. C.; Watson, A. D.; Gamp, E.; Hagen, K. S.; Edelstein, N.; Frankel, R. B.; Holm, R. H. *J. Am. Chem. Soc.* **1984**, *106*, 5941. A typical example, the Mössbauer spectrum of a high-spin triiron(III) complex in an external magnetic field, is shown in Figure 6 of this reference.

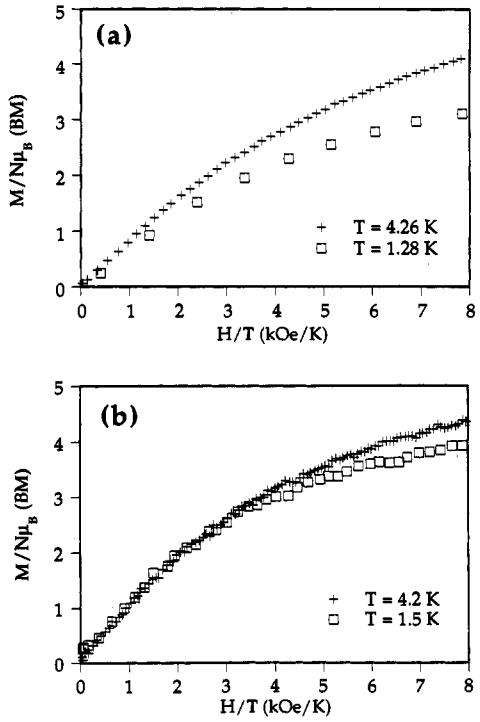

Figure 10. Initial data points of μ_B/cluster versus H/T for (a) **1** and (b) **2**. In b, a small effective superparamagnetic region is observed for $H/T < 4$ (kOe/K) in which the plots for $T = 1.5$ K and $T = 4.2$ K are congruent. In a, no such region is defined. The lack of congruence indicates, however, that this also is not a simple paramagnet.

magnetism[68,69] predict that there are regions in H/T parameter space for which either superparamagnetic or antiferromagnetic contributions to the magnetization dominate. In Figure 10, we plot M versus H/T for compounds **1** and **2**, from which it can be seen that there is a predominant superparamagnetic region, but only at $H/T < 4$, for the $\{Fe_{17}\}$ cluster. For $\{Fe_{16}Mn\}$, no such region was observed over the experimentally accessible temperatures nor was there simple paramagnetic behavior. We attribute these results to the extremely small size, ~10 Å diameter, of the magnetic cores of these clusters. Mössbauer spectroscopy, with its short characteristic measuring time of $\tau_m \sim 10^{-8}$ s, can thus be seen to afford a probe into the magnetic microstructure of these nanomaterials that is more powerful than magnetization measurements, for which τ_m is 10 s or longer.

In summary, although the onset of collective magnetic interactions has been demonstrated for the heptadecanuclear clusters described here, complete crossover to classical bulk magnetic behavior has not yet occurred. Quantum size effects dominate, placing these molecules at the boundary of molecular and bulk magnetic materials.

Comparisons with Iron–Apoferritin Complexes. The iron nucleation process in ferritins begins with molecular complexation of iron by apoferritin and leads ultimately to an oxo–hydroxo polyiron(III) solid-phase core. It thus provides, in a bioinorganic framework, an opportunity to investigate a topic of great current interest, namely, the boundary between discrete molecular structures and infinite arrays of the solid state.[13,70-72] Theoretical studies[73-76] of the electronic and magnetic properties of metallic clusters indicate that the onset of solid-state behavior, for example the emergence of a conduction band or collective magnetic phenomena, may occur when there are as few as 10 metal atoms in the cluster.[77-81]

Table 3. Mössbauer Parameters for $[Fe_{16}MnO_{10}(OH)_{10}(O_2CPh)_{20}]$ (**1**), $[Fe_{16}FeO_{10}(OH)_{10}(O_2CPh)_{20}]$ (**2**), **4** (ferric center), Fe(III)–apoferritin Complex, and Horse Spleen Ferritin

sample	isomer shift[a] (mm s^{-1})	T[b] (K)	ΔE_Q (mm s^{-1})	T_B[c] (K)	H_{hyp} (kOe)
1	0.51	80	0.77	4	400[d]
2	0.48	20	0.82	2	380[d]
4 (ferric center)[27]	0.47	20	0.74	4	497[d]
Fe(III)–apoferritin[82]	0.48	91	0.78	7	447
ferritin[82]	0.46	91	0.70	38	487

[a] Isomer shifts are referenced to metallic iron at room temperature. [b] Temperature at which the measurement was made, unless otherwise noted. [c] Blocking, or for the clusters, effective blocking (T_B') temperature (see text). [d] $T \sim 2$ K.

The Mössbauer parameters for **1**, **2**, and the ferric centers in **4** are compared to those of the clusters formed at the initial stages of iron complexation and nucleation in the ferritin core under conditions of limited Fe(II) concentrations and the parameters for the fully developed ferritin cores in Table 3. Compared to fully formed ferritin oxo–hydroxo–iron cores, the synthetic structures **1** and **2** and the polynuclear Fe(III) complexes with the protein exhibit similar quadrupole splittings, lower T_B values, and reduced hyperfine fields.

Conclusions

The major findings of this research may be summarized as follows.

(i) A series of three closely related compounds of general formula $[Fe_{16}MO_{10}(OH)_{10}(O_2CPh)_{20}]$, where M = Mn, Fe, or Co, has been synthesized from basic iron benzoate starting materials and a salt of the divalent metal ion M in acetonitrile solution.

(ii) The structures of the compounds are centrosymmetric with the M atom sitting on the center at a site that corresponds to the sharing of two Fe_3MO_4 cubes at a common corner. Overall, the $[Fe_{16}MO_{10}(OH)_{10}(O_2CPh)_{20}]$ structures may be formally constructed by fusion of two fragments of the previously reported compound $[Fe_{11}O_6(OH)_6(O_2CPh)_{15}]$. This analysis has permitted derivation of a scheme for formal construction of even larger clusters which are predicted to have the general formula M_n-$Fe_{5n+11}O_{4n+6}(OH)_{4n+6}(O_2CPh)_{5n+15}$, where n = 1, 2, 3, etc.

(iii) Magnetic susceptibility and high-field magnetization measurements of the $\{Fe_{16}Mn\}$ and $\{Fe_{17}\}$ clusters reveal complicated behavior characteristic of a high density of thermally accessible magnetic states. Neither the low-temperature nor high-field limiting magnetic moment was achieved at 1.5 K and fields up to 200 kOe. These properties are indicative of compounds at the molecular/solid-state boundary.[13]

(iv) A detailed analysis of the zero-field and magnetic Mössbauer spectra of the $\{Fe_{16}Mn\}$ and $\{Fe_{17}\}$ compounds reveals many similarities to the polyiron oxo clusters that form when iron(II) is added to apoFt and subsequently exposed to dioxygen. Included is the unusual observation of the onset of superpara-

(67) Bean, C. P.; Jacobs, I. S. *J. Appl. Phys.* **1956**, *27*, 1448.
(68) Néel, L. *J. Phys. Soc. Jpn.* **1962**, *17*, Suppl. B-1, 676.
(69) Mohie-Eldin, M. E.; Frankel, R. B.; Gunther, L. *J. Magn. Magn. Mater.* **1994**, *134*, in press.
(70) Sessoli, R.; Gatteschi, D.; Caneschi, A.; Novak, M. A. *Nature* **1993**, *365*, 141.
(71) Gatteschi, D.; Pardi, L.; Sessoli, R. *Mater. Sci.* **1991**, *17*, 7.
(72) Gatteschi, D.; Caneschi, A.; Pardi, L.; Sessoli, R. Submitted for publication.
(73) Messmer, R. P. *Surf. Sci.* **1981**, *106*, 225.
(74) Marzke, R. F. *Catal. Rev. Sci. Eng.* **1979**, *19*, 43.
(75) Koutecky, J.; Fantucci, P. *Chem. Rev.* **1986**, *86*, 539.
(76) Pastor, G. M.; Dorantes-Davila, J.; Bennemann, K. H. *Physica* **1988**, *B149*, 22.
(77) Messmer, R. P.; Knudson, S. K.; Johnson, K. H.; Diamond, J. B.; Yang, C. Y. *Phys. Rev. B* **1976**, *13*, 1396.
(78) Lee, K.; Callaway, J.; Dhar, S. *Phys. Rev.* **1984**, *B30*, 1724.
(79) Yang, C. Y.; Johnson, K. H.; Salahub, D. R.; Kaspar, J.; Messmer, R. P. *Phys. Rev.* **1981**, *B24*, 5673.
(80) Baetzold, R. C.; Mack, R. E. *J. Chem. Phys.* **1975**, *62*, 1513.
(81) Demuynck, J.; Rohmer, M.-M.; Strich, A.; Veillard, A. *J. Chem. Phys.* **1981**, *75*, 3443.
(82) Yang, C.-Y.; Meagher, A.; Huynh, B. H.; Sayers, D. E.; Theil, E. C. *Biochemistry* **1987**, *26*, 497.

magnetic-like behavior, which occurs at an effective blocking temperature of 2–4 K, further emphasizing the solid-state type properties of these clusters.

Acknowledgment. We are grateful to the National Institute of General Medical Sciences and the National Science Foundation for support of this research. Additional support was provided by the National Institutes of Health (National Research Service Award CA-59223, L.E.P., and Training Grant CA-02112, R.L.R.) and the Office of Naval Research, Program on Cluster Science and Dynamics (contract N00014-89-J-1779, G.C.P.). V.McK. is grateful to the University of Canterbury, Christchurch, New Zealand, for granting her leave. The high-field magnetization measurements were made with the assistance of E. McNiff at the MIT High Field User's Facility, which is supported by the NSF. We also thank Dr. J. G. Bentsen for carrying out the EPR measurements.

Supplementary Material Available: Tables of atomic positional and thermal parameters and full lists of interatomic distances and angles for compounds **1**, **2**, and **3**, FTIR spectra for **1**, **2**, **3**, and $\{Fe_{11}\}$, and Mössbauer spectra for **1** and **2** (69 pages). This material is contained in many libraries on microfiche, immediately follows this article in the microfilm version of the journal, and can be ordered from the ACS; see any current masthead page for ordering information.